a white paper submitted to the Voyage 2050 ESA call

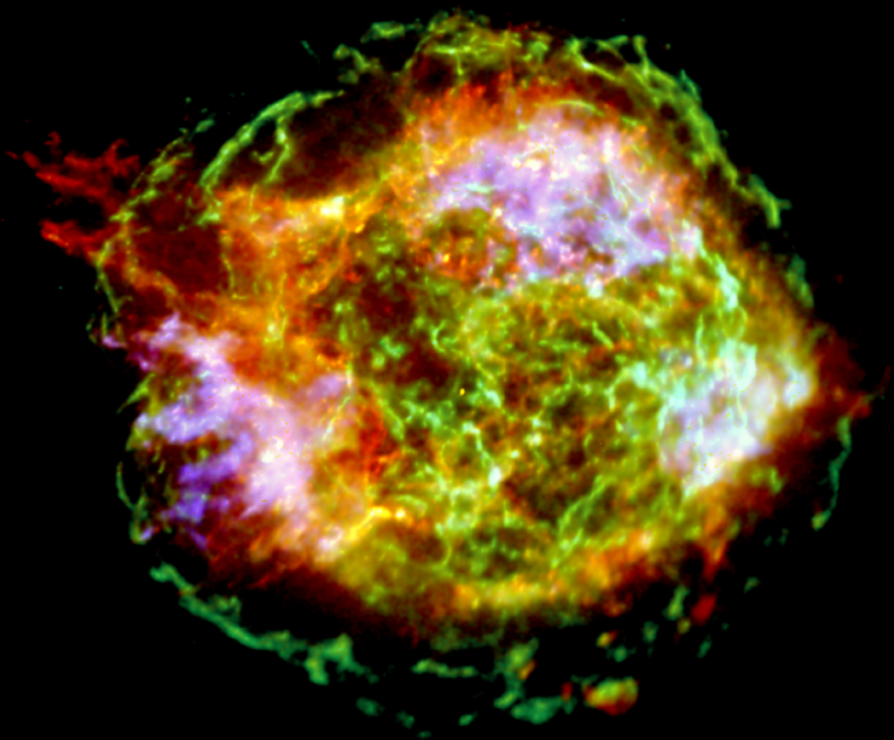

Understanding the origin of the positron annihilation line and the physics of the supernova explosions

Contact Scientist: Filippo Frontera

Physics and Earth Science Department - University of Ferrara, Italy

Observatory of Astrophysics and Space Sciences - INAF, Bologna, Italy

e-mail: frontera@fe.infn.it

Mobile: (+39) 334-1019.449

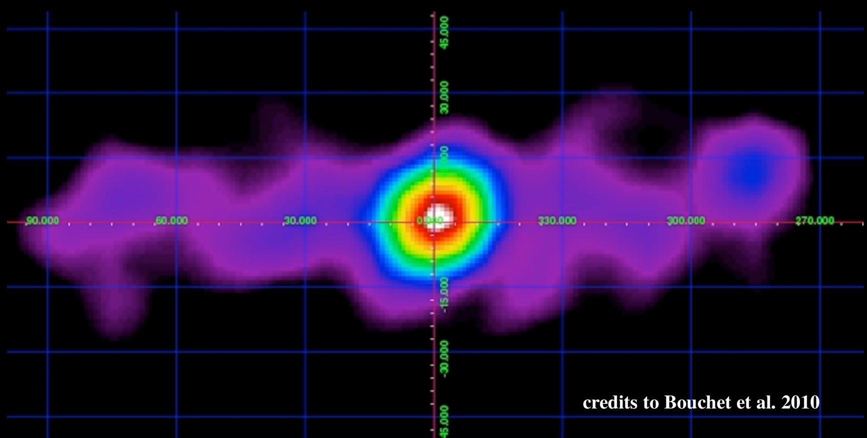

Proposing team:

F. Frontera[1,2], E. Virgilli[1], C. Guidorzi[1], P. Rosati[1], R. Diehl[3], T. Siegert[4], C. Fryer[5], L. Amati[2], N. Auricchio[2], R. Campana[2], E. Caroli[2], F. Fuschino[2], C. Labanti[2], M. Orlandini[2], E. Pian[2], J. B. Stephen[2], S. Del Sordo[6] C. Budtz-Jorgensen[7], I. Kuvvetli[7], S. Brandt[7], R. M. Curado de Silva[8], P. Laurent[9], E. Bozzo[10], P. Mazzali[11], M. Della Valle[12]

[1] Department of Physics and Earth Sciences, University of Ferrara, Via Saragat 1, I-44122 Ferrara, Italy

[2] Observatory of Astrophysics and Space Sciences, National Institute of Astrophysics (INAF), Via Gobetti 101, 40129 Bologna, Italy

[3] Max Planck Institut für extraterrestrische Physik Giessenbachstr.1, Postfach 1312, D-85741 Garching, Germany

[4] Center for Astrophysics and Space Sciences, University of California, San Diego, 9500 Gilman Dr, La Jolla, CA 92093, USA

[5] Los Alamos National Laboratory - New Mexico 87545, USA

[6] Institute Space Astrophysics and Cosmic Physics, INAF, Palermo, Italy

[7] DTU Space, Copenhagen, Denmark

[8] University of Coimbra, Coimbra, Portugal

[9] IRFU, CEA, Universite Paris-Saclay, F-91191 Gif-sur-Yvette, France

[10] Department of Astronomy, University of Geneva, CH-1290 Versoix, Switzerland;

[11] John Moores University, Astrophysics Research Institute, Liverpool, UK

[12] Osservatorio Astronomico di Capodimonte, INAF, Napoli, Italy

Abstract

Nuclear astrophysics, and particularly nuclear emission line diagnostics from a variety of cosmic sites, has remained one the least developed fields in experimental astronomy, despite its central role in addressing a number of outstanding questions in modern astrophysics. Radioactive isotopes are co-produced with stable isotopes in the fusion reactions of nucleosynthesis in supernova explosions and other violent events, such as neutron star mergers. The origin of the 511 keV positron annihilation line observed in the direction of the Galactic Center is a 50-year-long mystery. In fact, we still do not understand whether its diffuse large-scale emission is entirely due to a population of discrete sources, which are unresolved with current poor angular resolution instruments at these energies, or whether dark matter annihilation could contribute to it. From the results obtained in the pioneering decades of this experimentally-challenging window, it has become clear that some of the most pressing issues in high-energy astrophysics and astro-particle physics would vastly benefit from a significant progress in the observational capabilities in the keV-to-MeV energy band. Current instrumentation is in fact not sensitive enough to detect radioactive and annihilation lines from a wide variety of phenomena in our and nearby galaxies, let alone study the spatial distribution of their emission. In this white paper, we discuss how unprecedented studies in this field will become possible with a new low-energy gamma-ray space experiment, called ASTENA (Advanced Surveyor of Transient Events and Nuclear Astrophysics), which combines new imaging, spectroscopic and polarization capabilities. In a separate white paper (Guidorzi et al.), we discuss how the same mission concept will enable new groundbreaking studies of the physics of Gamma Ray Bursts and other high-energy transient phenomena over the next decades.

1 Introduction

Nuclear science is key to understanding the energy that makes stars and supernovae shine, as well as the synthesis of the variety of chemical elements that evolved from the H-He mix left behind after the big bang. Despite its central role however, nuclear astrophysics has mostly remained a theoretical field, rather than an experimentally-confirmed science. It is in fact one of the most challenging and least developed fields of astronomy. The limited sensitivity and imaging capabilities of the gamma–ray instrumentation flown thus far has limited nuclear astrophysics studies only to the brightest nearby sources. This suggests that a large discovery space could be opened in this field by expanding the experimental frontier. Among the most relevant open issues of astro-particle physics today is certainly the origin of the 511 keV positron annihilation line from the Galactic bulge region and whether the seemingly diffuse emission is made up of a population of discrete unresolved sources. Another long-outstanding issue is a detailed understanding of the physical processes that shape the explosion of Type-Ia and core-collapse supernovae, which again could not benefit from the poorly-developed domain of nuclear astrophysics. Specifically, Type-Ia SN are the most important distance indicators on cosmological scales, thanks to an empirical relation (the Phillips law, Phillips 1993), that links their luminosity at maximum with the post-peak decline rate, thus making SN-Ia good standard candles. A landmark experimental progress in this field would make nuclear line diagnostics an essential tool to develop self-consistent physical models of SN-Ia light curves, which will lead to understand the nature of the current observed scatter and their behaviour as standard candles. More generally the exponential fading exhibited by SN light curves is an indirect evidence of elements in making (Clayton, 1969). Nuclear gamma-ray astronomy carried out with the proposed mission concept ASTENA would provide a direct experimental confirmation of explosive nucleosynthesis theory, both in the continuum and in the lines emitted following the decay of ^{56}Co, ^{56}Ni, ^{44}Ti and ^{56}Fe.

2 The 511 keV positron annihilation line from the Galactic Center region

A recollection of the discovery and early observations of the 511 keV line can be found in the historical review on hard X–/soft gamma–ray astronomy by Cavallari and Frontera (2017). For a recent review including the astrophysical implications, see Prantzos et al. (2011). The two fundamental questions are: 'Where do the positrons come from?' and 'Why does the emission appear so different to our other views of our Galaxy?' – this is generally known as 'the positron line puzzle'. In the following, we will provide a short overview of the findings over the last 50 years and describe the potential of, and need for, a sub-arcminute telescope to solve the controversy on the 511 keV emission.

2.1 Emission morphology – Diffuse or not?

Discovered by Johnson et al. (1972) in a balloon flight in 1970, refined by Leventhal et al. (1978), it was confirmed in another flight in 1979 (Leventhal et al., 1980). During the first 25 years of study, the line flux was found to be variable and sometimes undetected. In the late 1980s, the *Solar Maximum Mission* (SMM) consistently detected the 511 keV line at a flux level of 2.3×10^{-3} photons/(cm^2 s) (Share et al., 1990), compared to the upper limits of more balloon flights earlier in the decade (Leventhal et al., 1986), and with other balloons later (e.g. GRIS, Gehrels et al. 1991). With the satellite experiment OSSE on CGRO (Purcell et al., 1993), the line flux was found stable at a flux level of $\sim 10^{-3}$ photons/(cm^2 s), and the apparent variability was attributed to peculiar diffuse emission which was only partly captured by the different field of views of previous instruments (Albernhe et al., 1981; Lingenfelter and Ramaty, 1989). This earliest mapping of the 511 keV line emission was performed by Purcell et al. (1997) using CGRO/OSSE, WIND/TGRS (Teegarden et al., 1996), and SMM data. Unlike at other wavelengths, the emission was dominated by a central bulge, a probably truncated emission from the Galactic plane, and an enhancement at positive latitudes above the Galactic Center (GC). With INTEGRAL/SPI, the morphology became clearer over time, with a sole detection of the bulge after 1.5 years (Knödlseder et al., 2005), a possible asymmetric disk emission after 3 years (Weidenspointner et al., 2008), and the correction of these findings after 8 years (Bouchet et al., 2009), describing the 511 keV map with a shifted bulge and a low surface-brightness disk. With more than 10 years of INTEGRAL/SPI data, spectral positron annihilation features are detected with $\sim 70\sigma$ in the bulge and $\sim 12\sigma$ in the disk (Siegert et al., 2016b), with an angular resolution of $\sim 3°$. While OSSE's 'Galactic Positron Fountain' has never been confirmed, a new debate on whether the disk is actually thin or shows a large scale height is ongoing (Skinner et al., 2014; Siegert et al., 2016b). The bulge emission is now found as highly symmetric and can be described by a combination of two 2D Gaussians with a slight shift towards negative longitudes (Skinner et al., 2014), including a dominating component of about ~ 6 deg (FWHM), and a possible point source at the GC with a flux of $(0.8 \pm 0.2) \times 10^{-4}\,\mathrm{photons\,cm^{-2}s^{-1}}$. The most recent flux estimate for the entire Milky Way is $(2.7 \pm 0.3) \times 10^{-3}\,\mathrm{photons\,cm^{-2}s^{-1}}$, which converts to an annihilation rate (luminosity) of $\sim 5 \times 10^{43}\,\mathrm{e^+\,s^{-1}}$ (Siegert et al., 2016b). This number, if not steadily decaying from a much larger supply, must be sustained by one or more sources, which to date, are still unknown[1].

[1] The β^+-decay of ^{26}Al is believed to make about 10 % of the total flux, but a 'smoking gun' evidence for this candidate source is not yet found.

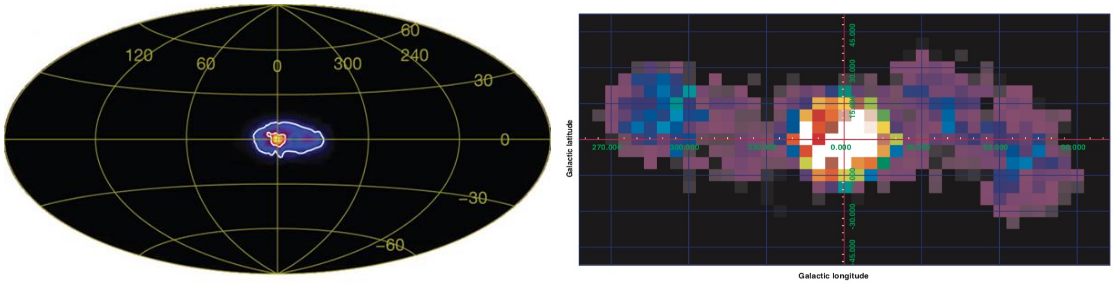

Figure 1: Sky map of the 511 keV positron annihilation line found with the *INTEGRAL* SPI telescope by Weidenspointner et al. (2008) (*left panel*) and by Bouchet et al. (2009) (*right panel*). According to Weidenspointner et al. (2008), the integrated fluxes in the negative ($-50 < l < 0$) and positive ($0 < l < 50$) longitude bands, within 10 deg of the Galactic plane, are $(4.3 \pm 0.5) \times 10^{-3}$ photons/(cm^{-2} s) and $(2.4 \pm 0.5) \times 10^{-3}$ photons/(cm^{-2} s), respectively. The integrated flux found by Bouchet et al. (2009) was consistent with that reported by Weidenspointner et al. (2008), but no asymmetry was found.

2.2 Candidate sources – Detecting sources in flagranti

Due to the seemingly asymmetric disk reported by Weidenspointner et al. (2008), an attempt was made to correlate the emission with the population of Low Mass X-ray Binaries (LMXRBs), dominating at $\gtrsim 10$ keV, as the distribution of then-known 71 LMXRBs appeared tantalizing (45 at negative longitudes, 26 at positive longitudes). While the asymmetry was not confirmed (see Fig. 1, from Weidenspointner et al. (2008) and Bouchet et al. (2009)), LMXBs may still have a large contribution to the positron content of the Milky Way. As a result of annihilation of positrons produced in e^+-e^- pair-dominated jets (Celotti and Blandford, 2001) of black-hole systems or of γ–γ interactions in the inner regions of high–temperature/high-density accretion disks of XRB systems, the population of XRBs can potentially account for all the positrons seen to annihilate. This microquasar-511 keV conjecture is supported by detections of thermal pair plasma emission from three sources in outburst: 1E 1740.7-2942, "the Great Annihilator" (Bouchet et al., 1991), Nova Musca (Goldwurm et al., 1992), and V404 Cygni (Siegert et al., 2016a) – all of which have been debated though. Also given the thousands of Chandra sources revealed within only 17×17 arcmin around Sgr A* (Hailey et al., 2018), the possibility that the 511 keV line is due to a superposition of discrete sources remains an attractive solution.

Sgr A* itself is also a prominent candidate source in this context, either by a pair-dominated jet, 'calming down' from past AGN activity, or triggering a star burst event several million years ago (Prantzos et al., 2011; Alexis et al., 2014). The possibility of a point-like source in the GC (Skinner et al., 2014; Siegert et al., 2016b) requires confirmation, and still opens intriguing possibilities concerning the positron puzzle. Given the low angular resolution (2.7°) of SPI (Vedrenne et al., 2003) and other experiments, Bandyopadhyay et al. (2009) recall that *"from the data it is unclear whether the emission is truly diffuse, or if it originates either from a single discrete source (e.g. SgrA* or 1E 1740.7-2942 [...]) or from a small number of discrete but unresolved sources."*. Within 2.7° at a distance of 8.1 kpc, a region as large as 400 pc fits into only one PSF of SPI. This size is reminiscent of the Central Molecular Zone, harbouring not only XRBs, but also molecular gas in which positrons may prefer to annihilate, as well as a dense cluster of stars – the nuclear star cluster. The population of flaring M- to G-type stars may in fact provide a complete solution as well: Bisnovatyi-Kogan and Pozanenko (2017) estimated that the $\sim 10^{11}$ stars in the Milky Way show a quasi-persistent 511 keV flux from intermittent stellar flares, producing pions and β^+-unstable nuclei. The sheer number of stars may appear as a diffuse flux of the order of $10^{-3}\,\mathrm{ph\,cm^{-2}\,s^{-1}}$ at 511 keV and would readily explain the bulge emission. The nuclear stellar cluster as well as a large number of Milky Way's globular clusters would stand out of the otherwise diffuse glow and provide direct evidence for these type of scenarios. With arcmin resolution, it would furthermore be possible to distinguish among mildly relativistic, quiescent XRB outflows (Bartels et al., 2018) or stellar flares as the latter would directly follow the globular cluster's radial profile.

A possible explanation for the positron puzzle are the β^+-decays from radioactive ejecta of massive stars and their core-collapse supernovae (CCSNe), as well as of white dwarf systems in classical novae (CNe) or thermonuclear type Ia supernovae (SNe Ia). Here, the most important nuclei are ^{26}Al ($T_{1/2} \approx 717$ kyr; 1809 keV line; massive star winds, CCSNe, CNe), ^{44}Ti ($T_{1/2} \approx$ 60 yr; 68, 78, 1157 keV lines; CCSNe, SNe Ia, e.g. Sim and Mazzali 2008), ^{22}Na ($T_{1/2} \approx 2.75$ yr; 1275 keV line; CNe), and ^{56}Co ($T_{1/2} \approx 0.2$ yr; 847, 1238 keV lines[2], CCSNe, SNe Ia, e.g. Clayton and Hoyle 1974). While the latter is the main energy producer for the light curves of SNe Ia and consequently the line-of-sight escape from the main sources is very uncertain (e.g. Milne et al., 1999), all the decay positrons have in common that they first have to slow down to explain the measured signal: β^+-decay typically emits $\lesssim$ MeV positrons, but the line shape suggests positrons at eV energies (e.g. Churazov et al., 2005; Jean et al., 2006; Siegert et al., 2016b; Siegert et al., 2019). This slowing down is connected to the propagation of cosmic-ray positrons, and the interplay of the environmental conditions near the initial source and the properties of the interstellar medium between source and region of annihilation. This becomes even more important when pair-produced positrons from interactions of high-energy photons in the strong magnetic fields of pulsars are considered (e.g. Daugherty and Harding, 1983). In addition to these away-from-the-source scenarios, CNe systems are expected to show a short, ~ 1 hr, flash or 511 keV radiation from the decay of short-lived ^{13}N and ^{18}F, which however has never been detected. In order to distinguish between either of these scenarios, or to establish whether more sources are required to explain the total signal, superb line sensitivity as well as unprecedented angular resolution is required. The focusing telescope part of the ASTENA mission concept we are proposing here (see Fig. 17), will have a 511 keV sensitivity of $\sim 7 \times 10^{-6}$ in 1 Ms, with which it will be possible: 1) to detect 511 keV emission from SNe Ia up to a distance of ~ 10 Mpc to directly measure the escape fraction of positrons, 2) to see CNe flashes up to 5 kpc and detect the decay positrons from ^{22}Na up to 1 kpc, 3) to unravel the annihilation regions in the vicinity of massive stars (e.g. Cygnus OB associations), 4) to discover the late light curve heating of CCSNe by measuring positron annihilation from ^{44}Ti in Cassiopeia A, and 5) to possibly detect extragalactic emission regions of 511 keV in the LMC and M31.

Ultimately, with our proposed instrumentation one will be able to discriminate between the diffuse vs. discrete origin of the 511 keV line, by performing a scan of selected regions near the GC, with a telescope with a much higher sensitivity and angular resolution than any current or planned instrumentation.

2.3 The 511 keV line and the quest for dark matter

As summarised above, the pure astrophysical explanation of the 511 keV diffuse emission extending over $\sim 10\,\mathrm{deg}^2$ around the GC is far from being clear, and it remains a challenge to explain the spectrum, intensity and morphology of the INTEGRAL signal with candidate sources (see Prantzos et al. 2011 for a review). Therefore, since the first detailed map of the GC by INTEGRAL/SPI was released (Fig.1), many studies have tried to establish whether annihilation or decay of dark matter (DM) particles can possibly contribute to the 511 keV

[2] From the decay of ^{56}Ni ($T_{1/2} \approx 6$ d; 158, 812 keV lines).

line production (e.g. Boehm et al. 2004; Finkbeiner and Weiner 2007, see also Bœhm 2009). Even though the central slope of the dark matter density profile of our galaxy is still not well known matter, the number density of annihilating positrons depends on the square of the DM number density, which necessarily peaks near the GC. These first and more recent studies (e.g. Chan and Leung 2018) have constrained the possible annihilation channels, annihilation cross sections, and dark matter mass range, finding that specific models with MeV-to-GeV masses can reproduce the 511 keV signal, and at the same time being consistent with the relic density of DM from cosmological observations. Other studies have instead found MeV annihilating relic dark matter inconsistent with cosmological data (Wilkinson et al. 2016). It is clear that the lack of knowledge of the physics of DM, makes these predictions quite speculative, especially when the contribution of discrete, currently unresolved sources to the 511 keV extended signal, is still not known. By disentangling the point source contribution from the 511 keV emission with highly sensitive, sub-arcminute resolution maps, one will obtain a firm measurement of a possible excess of positrons in the galactic bulge. This will in turn significantly narrow down the range of DM physical parameters consistent with such excess, or lack thereof.

3 Line emission from radioactive nuclei produced in supernova explosions of types Ia and core-collapse

3.1 Type Ia SNe

SN Ia are the outcome of the thermonuclear explosion of either a single Carbon/Oxygen white dwarf with a mass near the Chandrasekhar limit in a close binary system or a pair of merging white dwarfs. The burning of the Carbon/Oxygen mixture provides the required kinetic energy, while the decay of ^{56}Ni $\longrightarrow$ ^{56}Co with a half–life of 6.1 days and that of ^{56}Co $\longrightarrow$ ^{56}Fe, with a half–life of 77.7 days, power the optical light curve, as shown by the SN2014J observations with *INTEGRAL*, 50 and 100 days after the explosion (Churazov et al., 2014; Diehl, 2015), in agreement with theoretical expectations, e.g., by Kuchner et al. (1994). Between 50 and 100 days after the explosions, γ rays leak out from the supernova interior, and could be observed with INTEGRAL. Using the SPI and the IBIS/ISGRI telescopes aboard *INTEGRAL*, Churazov et al. (2014) reported the detection of the ^{56}Co lines at energies of 847 keV and 1238 keV and a γ–ray continuum in the 200–400 keV band. Detection of the ^{56}Co γ rays establishes directly that 0.6 ± 0.1 solar masses of radioactive ^{56}Ni were synthesized during the explosion (Churazov et al., 2014; Diehl, 2015). On the other side, about three weeks after explosion of this same SN, from data of the SPI telescope, Diehl et al. (2014) reported the detection of both the 158 and 812 keV lines from the ^{56}Ni decay, with intensities of $(1.10{\pm}0.42){\times}10^{-4}$ photons cm^{-2}s^{-1} and $(1.90{\pm}0.66){\times}10^{-4}$ photons cm^{-2}s^{-1} , respectively. This evidence of radioactive ^{56}Ni near the surface, later confirmed by Isern et al. (2016), points to explosion asymmetries, if not an initial, triggering, surface explosion (see discussion in Diehl et al., 2014).

Understanding the physical processes leading to explosions of type Ia SNe is very important, given that SN Ia are used as distance indicators at cosmological scale, extrapolating the empirical Phillips correlation far beyond the established nearby redshift regime. The Phillips relation between maximum luminosity and post–peak decline rate allows one to standardize the absolute luminosity and correct for individual SN Ia properties, as shown by reducing the light peak dispersion of the observed SNe from 1.5 mag to 0.1–0.2 mag. A robust physical modeling of the Phillips law could further improve the accuracy in the distance measurement, as, e.g., effects of different metallicity on the explosion would be included in a truly-physical model. Given the primary role of ^{56}Ni and its products in powering the light curve, the mea-

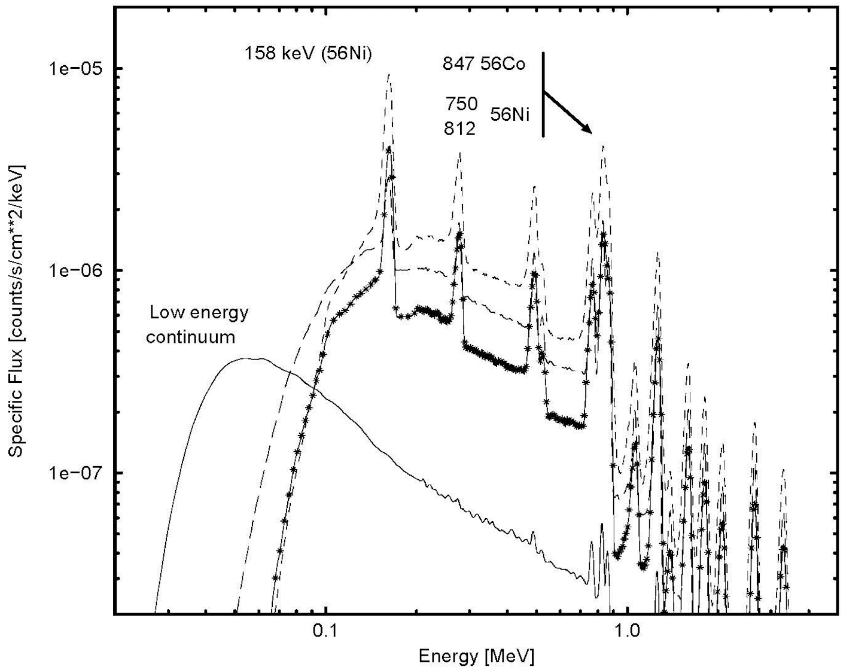

Figure 2: Expected gamma–ray spectrum of a SN Ia at 20 days from the explosion. The different curves refer to different possible explosion mechanisms (deflagration, detonation and delayed detonation). Reprinted from Gómez-Gomar et al. (1998).

surement of SNe Ia gamma–ray lines and continuum spectrum is a crucial diagnostic tool to understand the physics of the explosion and its evolution (Gómez-Gomar et al., 1998).

At early times from the explosion (see Fig. 2), the spectrum is dominated by the ^{56}Ni main lines (158 keV and 812 keV) and from the 847 keV and 1238 keV lines due to the radioactive ^{56}Co. The strongest lines are the 158 keV line and the 812 and 847 keV lines. However, given the limited energy resolution of gamma–ray detectors, it is difficult to separate the last two lines. Thus, for the study of the early evolution of the SNe Ia, the study of the 158 keV offers the best approach.

The strength of the gamma-ray spectra depends on the mass and velocities of the ejecta, nickel mass and distribution. Figure 3 shows the diversity of gamma-ray lines on these explosion properties. A direct access to the total flux and line features will provide a novel powerful tool to measure these physical properties, thus probing the nature of the thermonuclear engine behind these supernovae.

In Fig. 4, we show the 158 keV line detected with *INTEGRAL* from SN2014J (Diehl et al., 2014) with an exposure time of 150 ks (Diehl et al., 2014). The estimated line intensity of $(1.1 \pm 0.4) \times 10^{-4}$ photons cm^{-2}s^{-1} corresponds to a detection confidence level of 2.5σ. For comparison, *ASTENA* NFT will reach a 3σ sensitivity at the same energy (see Fig. 17) of approximately 10^{-6} photons cm^{-2}s^{-1} in only 1 ksec observations.

As a result, *ASTENA* NFT will be capable to detect lines from SNe that synthesize lower masses of ^{56}Ni than those found near the surface of SN2014J (0.06 M$\odot$, Diehl et al. 2014, D = 3.3 Mpc), or to detect lines from SN Ia at greater distances. Given the significantly higher sensitivity and angular resolution of ASTENA, we also expect to be able to study the spatial distribution and the evolution of both line and continuum in the case of Galactic SNe. From theoretical estimates (Figs. 2 and 3) as well as observational evidence (SN2014J), we expect to significantly increase the number of SNe Ia that could be investigated in gamma–rays.

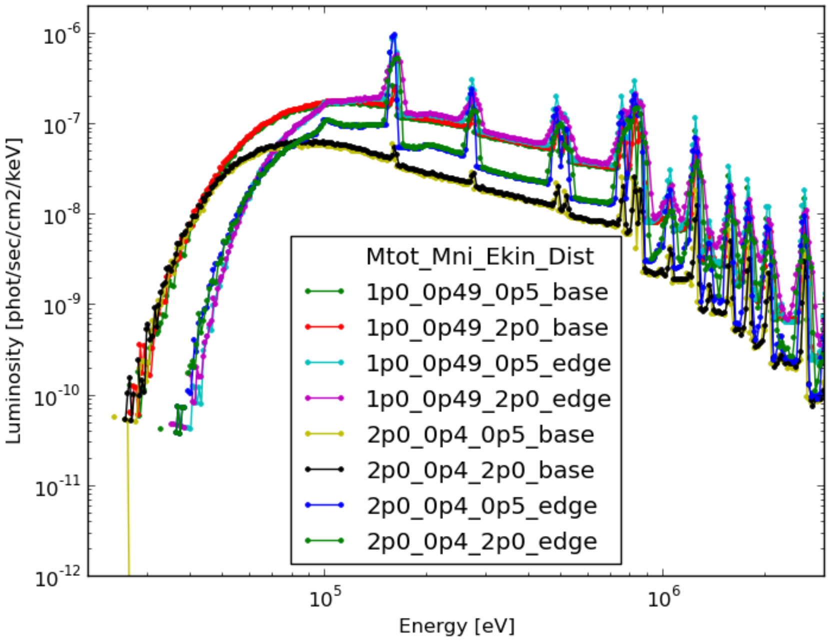

Figure 3: Expected gamma–ray spectrum of a SN Ia at 20 days from the explosion for a range of models where the explosion energy, total mass, nickel mass and its distribution are varied across the range of current explosion models (Hungerford et al., in preparation).

ASTENA's superior line sensitivity around 158 keV as well as the more than two orders of magnitude better continuum sensitivity around 200–400 keV would allow to follow-up between 50 and 200 SNe Ia per year, up to a distance of 120 Mpc ($z \lesssim 0.03$). Consequently, ASTENA would tremendously contribute to understanding the diversity of SNe Ia, their different explosion mechanisms (progenitor problem), as well as shed light on supernova cosmology.

3.2 Core Collapse SNe

In Core Collapse supernova explosions (CCSN; also called SN Ib/c or SN II) that result from collapses of massive stars at the end of their stellar evolution, one of the most diagnostic synthesized elements is ^{44}Ti. It decays according to the chain $^{44}\mathrm{Ti} \longrightarrow {}^{44}\mathrm{Sc} \longrightarrow {}^{44}\mathrm{Ca}$ with a half life of 58.9 ± 0.3 yrs (Ahmad et al., 2006) and direct emission of lines at 4.1, 67.9, 78.4, 511 and 1,157 keV, with relative brightnesses, i.e., average numbers of photons per decay, of 17.4%, 87.7%, 94.7%, 188.8% and 99.9%, respectively(Grebenev et al., 2012). Given the long decay time, these lines are visible at late times once the explosions are entirely transparent. Of the above lines, those so far clearly detected are the 67.9 and 78.4 keV and 1157 keV lines from Cas A, a SN exploded in 1671, with *BeppoSAX* (Vink et al., 2001), *INTEGRAL* (Renaud et al., 2006; Siegert et al., 2015) and *NuSTAR* (Grefenstette et al., 2014), and from the Type II SN1987A (Grebenev et al., 2012; Boggs et al., 2015). The integrated line intensity from Cas A is about 2×10^{-5} photons cm^{-2}s^{-1} . Thanks to the *NuSTAR* angular resolution (58 arcsec Half Power Diameter (HPD), Harrison et al. 2013), it has been possible for the first time to study the spatial distribution of the line across the remnant (Grefenstette et al., 2014, 2017). Concerning SN1987A whose distance is about 50 kpc, an estimate of a synthesized mass of ^{44}Ti of $(3.1 \pm 0.8) \times 10^{-4}$ $M_\odot$ was reported with *INTEGRAL* (Grebenev et al., 2012); the

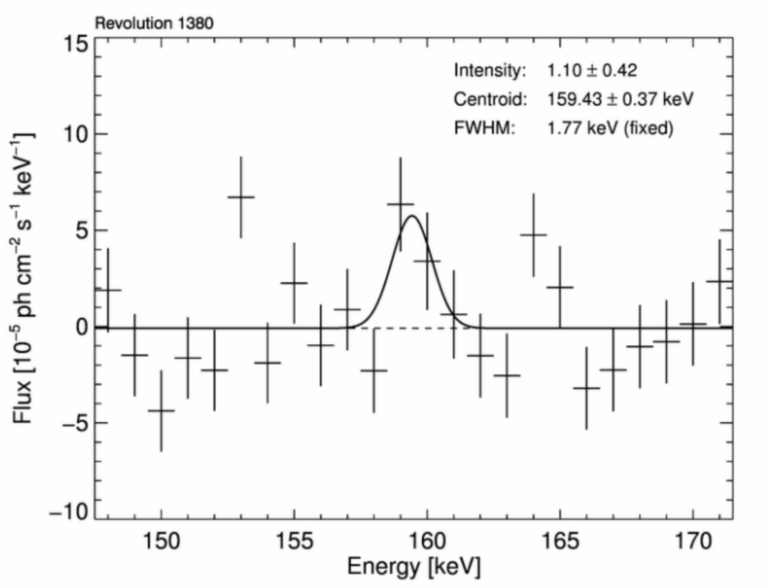

Figure 4: The 158 keV line due to the ^{56}Ni decay of SN2014J, as observed with 150.24 ks *INTEGRAL* SPI observations, 3 weeks after the explosion. The line intensity is given in 10^{-4} photons cm^{-2}s^{-1} units. Reprinted from Diehl et al. (2014).

NuSTAR measurement indicated that this intensity may have had a bias towards high values, the more-significant NuSTAR result is $(1.5 \pm 0.3) \times 10^{-4}$ M$_\odot$ (Boggs et al., 2015). Obtaining the yields for key metals detected in supernova remnants through X rays depends sensitively on the excitation of the atoms and out-of-equilibrium effects lead to large errors in the total abundances derived from X-ray observations. Photons from radioactive decay do not suffer from these systematics, providing a more-robust abundance measurement. Because ^{44}Ti is produced in the innermost supernova ejecta, it is an ideal probe of the explosion mechanism and potential asymmetries. The NuSTAR results (Grefenstette et al., 2014, 2017) are considered to be the strongest evidence for an intrinsic explosion asymmetry and clumpiness, and the convective-engine paradigm behind core-collapse supernovae. ^{44}Ti production is extremely sensitive to the exact nature of the explosion (shock strengths and densities) and, by measuring the spatial distribution of the ^{44}Ti yields relative to iron, we can probe these diagnostic metal ratios.

The NFT telescope aboard *ASTENA*, thanks to its angular resolution similar to that by *NuSTAR* and its higher sensitivity, will be capable to perform a more accurate spatial maps of the 67.9 and 78.4 keV lines across the remnant and to extend this study to other remnants.

In addition, in the rare event of a nearby neutron star merger event or a Galactic supernova, a host of new isotopes may be detected (Timmes et al., 2019). For neutron star mergers within 10 Mpc, scientists can probe the mass and composition produced of heavy r-process elements, firmly dictating the role that mergers play in r-process production and the robustness of their r-process composition (Korobkin et al., 2019; Wu et al., 2019). For Galactic supernovae, over 10 isotopes will be detected, some probing the stellar burning layers, others probing the explosion energy and mixing. These unique probes of cosmic explosions will dramatically improve our understanding of the progenitors and engines behind them.

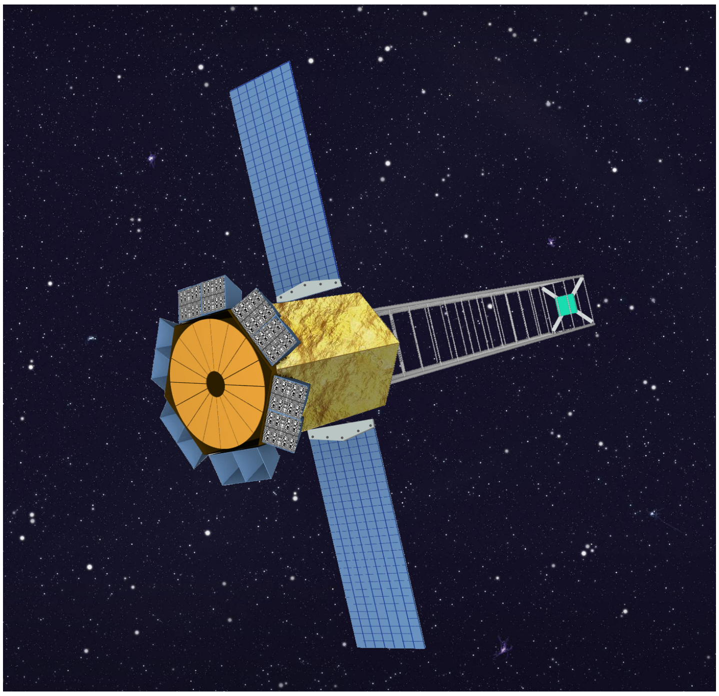

Figure 5: Artistic view of ASTENA in-flight configuration

3.3 Classical Nova Systems

CV systems are expected (see §2.2) on theoretical grounds to show a $\sim 1\,\mathrm{hr}$, flash of 511 keV radiation from the decay of short-lived ^{13}N and ^{18}F. Given a rate of $\sim 14 \pm 3$ nova/yr for the galactic bulge (Mroz, 2015) and the ASTENA sensitivity of $\sim 2 \times 10^{-5}$ at 511 keV in 100 ks, it will be possible to detect CN flashes up to 3 kpc for a handful of Novae per year and to detect the decay positrons from ^{22}Na up to $\lesssim 1\,kpc$.

4 ASTENA mission concept

The ASTENA in–flight configuration is shown in Fig. 5, while its main properties are reported in Table 1. The instrumentation on board consists of a Wide Field Monitor–Imaging Spectrometer (WFM-IS) with a 2 keV–20 MeV passband, and a Narrow Field Telescope (NFT) with a 50–600 keV passband. The WFM-IS consists of an array of 12 units, two units on each side of the hexagon surrounding the NFT. All the units are offset by 15 deg with respect to the axis of the NFT, as shown in Fig. 5. The NFT is a Laue lens telescope of about 3 m diameter and 20 m focal length. Part of the focal length (5 m) is inside the spacecraft and 15 m outside. The WFM-IS and the focal plane position sensitive detector (PSD) are inside the spacecraft at launch (see left and central panels of Fig. 6). The ASTENA spacecraft can be accommodated inside the fairing of a Soyuz or Vega C launcher (see right panel of Fig. 6).

4.1 WFM-IS units

Essentially, each detection unit (see Fig. 7) of the WFM-IS is a Position Sensitive Detector (PSD) surmounted by a coded mask at 70 cm distance. The mask is supported by 4 Aluminum slabs with, inside, for a portion of the height, a Tungsten layer about 500 μm thick.

Table 1: Main properties of the WFM-IS and of the NFT on board ASTENA.

	WFM-IS	**NFT**
Energy pass-band	2 keV – 20 MeV	50 – 600 keV
Total useful area[(a)]	$\sim$ 5800 cm^2 (< 30 keV)	
	$\sim$ 6700 cm^2 (30–150 keV)	7 m^2 (projected)
	$\sim$ 13800 cm^2 (>200 keV)	
Field of View	2 sr	4 arcmin
Angular resolution	6 arcmin	$\sim$ 30 arcsec HPD
Point source localization accuracy	1 arcmin (see text)	< 10 arcsec
Minimum Detectable Polarization	see Fig. 10	see Fig. 16

[(a)] Total geometric area through the mask or collimator.

4.1.1 The Position Sensitive Detector unit

The PSD unit consists of an array of 4×8 modules, each module consisting of 10 rows of hexagonal scintillator bars 4.5 mm between flats (205 bars per module), readout, on the top (toward the mask), by linear multi-anode Silicon Drift Detectors (SDDs) 0.4 mm thick, and, on the bottom, by hexagonal single anode SDDs 4.5 mm between flats (see Fig. 8). The functioning principle of this detector is similar to that adopted for the X-Gamma-ray Imaging Spectrometer (XGIS) aboard the THESEUS mission (Campana et al., 2018). It has the great advantage of a very broad passband (2 keV–20 MeV), a 3D position sensitivity to energy losses in the scintillator bars and a very low intrinsic background, given its similarity to the phoswich system (see, e.g., Frontera et al. 1997), in this case a "siswich" system as already demonstrated by Marisaldi et al. (2004, 2005). In the case of the WFM-IS units the top SDDs have 4 linear anodes for each scintillator bar (Fig. 8). This configuration allows to get a 1D position sensitivity of 1.25 mm, which is required to achieve, with a proper coded mask (see below), a Point Source Localization Accuracy (PSLA) of 1 arcmin at low energies (<30 keV). The hexagonal cross section of the bars is crucial to obtain the instrument unique polarimetric capabilities (see below). In the current design the scintillator material is CsI(Tl), but also other materials (like BGO and GAGG(Ce)) will be considered. Depending on the scintillator material, the length of the bars will be optimized also for exploiting the Compton interactions in different bars for the determination of the incident photon direction (see below).

4.1.2 Coded mask

Imaging capabilities of the WFM-IS are obtained by means of a double scale coded mask, one scale for the high energy photons (30–150 keV) that lose their energy in the scintillator bars, and another scale for the low energy photons (< 30 keV) that lose their energy in the SDD alone. The high energy mask is made of Tungsten 1 mm thick, while the low energy mask is made of stainless steel 0.5 mm thick. The high energy mask is a 43×41 element basic pattern of 10 x 10.1mm, with 79×79 of such elements for each detection unit, with 50% of open 2-dimension (2D) pixels, a Fully Coded Field of View (FCFOV) of 0.27 sr, and a Full Width at Zero Response (FWZR) of 2 sr. The expected Point Source Location Accuracy (PSLA) is approximately 5 arcmin for a 7 σ signal, and better for higher S/N signals.

Unlike the high energy mask, the low energy mask is 1-D (see left panel of Fig. 9), with

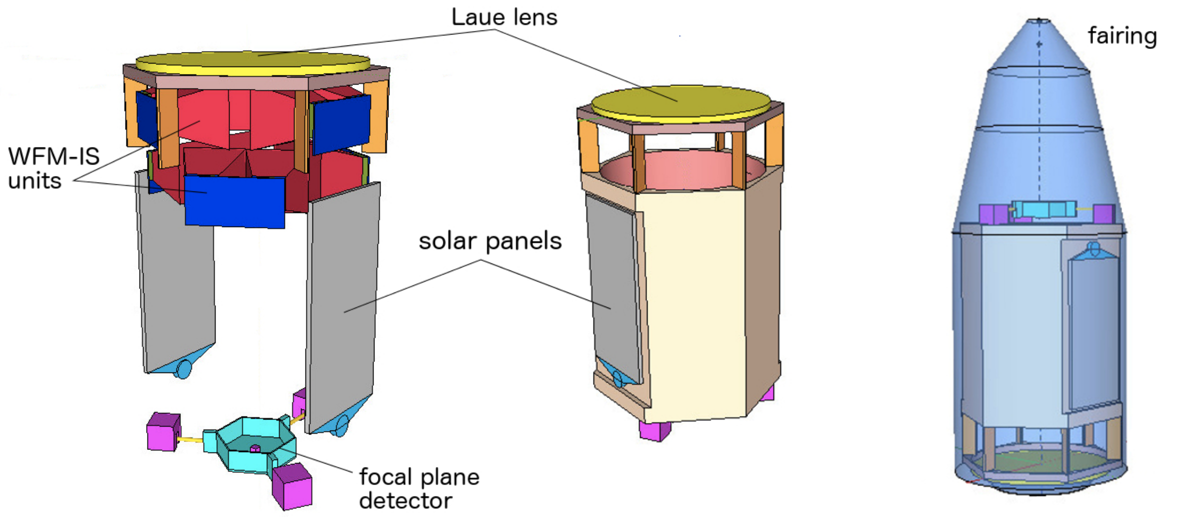

Figure 6: *Left panel*: A view of the inner accommodation of the ASTENA payload before the launch. *Central panel*: A view of the inner side of ASTENA spacecraft. *Right panel*: ASTENA satellite in the fairing of the Soyuz launcher. Also the fairing of the Vega C launcher can host ASTENA.

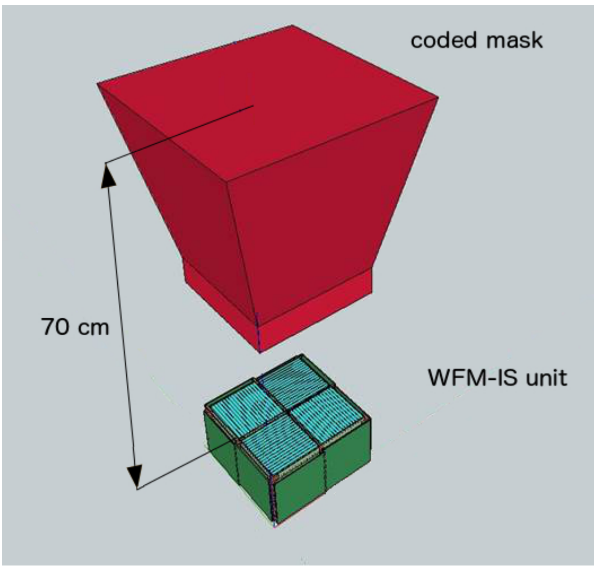

Figure 7: A schematic view of a WFM-IS unit.

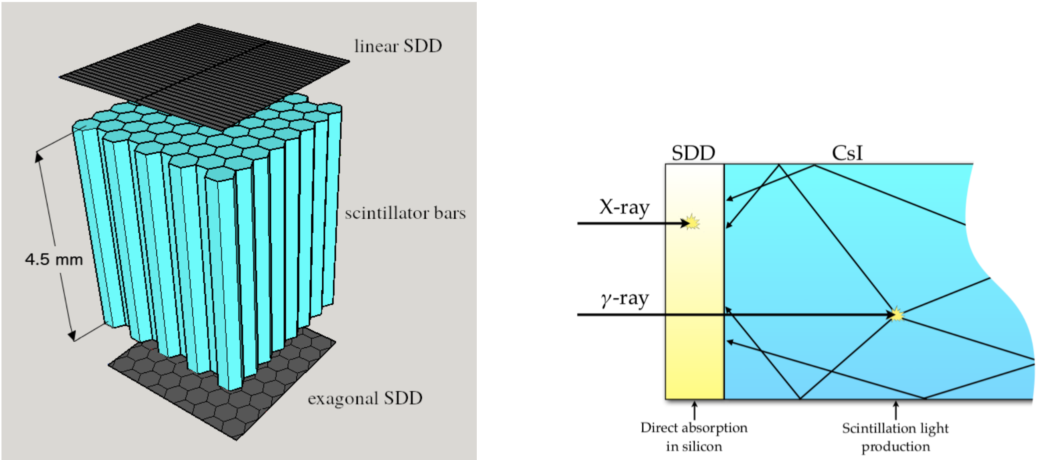

Figure 8: *Left*: Exploded view of a portion of a detection module of a WFM-IS unit. *Right*: working principle of a SDD coupled with a CsI scintillator crystal. The soft X-rays interact directly in the SDD while high energy photons pass through the SDD and are absorbed in the scintillator. Secondary photons are then detected with the SDD.

a throughput of $\sim$65%, so as to allow the combined 2D/1D mask pattern (see right panel of Fig. 9) to have a throughput of 50% at high energies and about 33% at low energies. With these properties, by positioning the 1-D directions of low energy scale of the mask of each pair of detectors (see Fig. 5) perpendicularly to each other, we can achieve a PSLA of 1 arcmin, which is required to perform NFT follow-up observations of sources discovered with the WFM-IS.

4.1.3 WFM-IS polarimetric capabilities

Thanks to the hexagonal cross section of the scintillator bars and the 3D position sensitivity of the detector, each detection unit can be used as a Compton scattering polarimeter. In Fig. 10, we show the Minimum Detectable Polarization at 3σ level in the case of a GRB of 20 s duration and 2 different fluences. The assumed spectrum is a Band law with low-energy photon index $\alpha = 1.0$, high energy photon index $\beta = 2.3$ and peak energy of the $EF(E)$ spectrum equal to 300 keV.

4.1.4 WFM-IS continuum sensitivity

Considering the throughput of the coded mask, the geometric area of the WFM-IS through the mask is $\sim$ 5800 cm^2 below 30 keV and 6700 cm^2 in 30–150 keV. At higher energies the mask is transparent to the radiation therefore the on-axis area is about 1.4 m^2. Assuming the background level expected for a nearly equatorial orbit, Figure 11 shows the WFM-IS continuum sensitivity as a function of the exposure time for a source in the FOV of the NFT.

4.2 Narrow Field Telescope, NFT

As mentioned above, the NFT is based on a broad band (50–600 keV) Laue lens with $\sim$ 3 m diameter and 20 m focal length (see sketch in the left panel of Fig. 12), with a Position Sensitive Detector (PSD) in the focal plane. We separately discuss both, Laue lens and PSD.

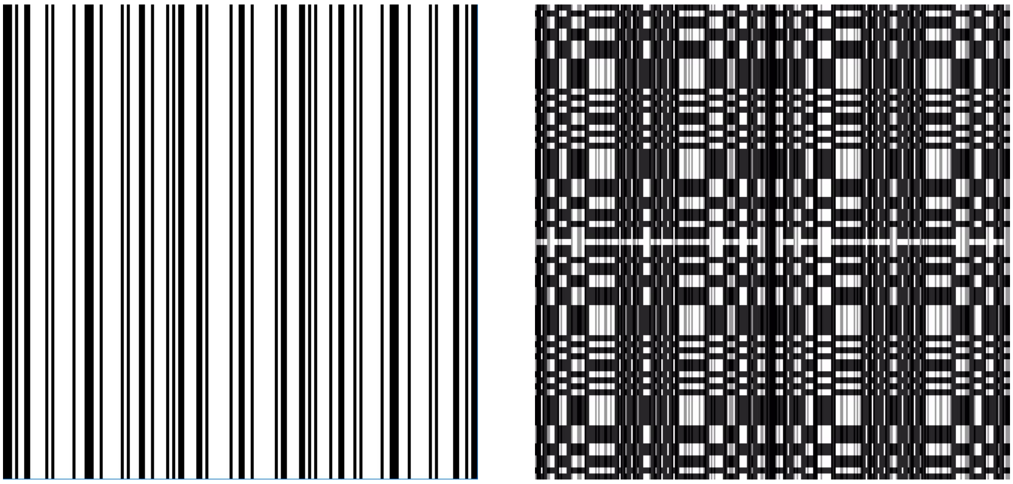

Figure 9: *Left*: Top view of the 1-D low energy coded mask. *Right*: top view of the double scale coded mask.

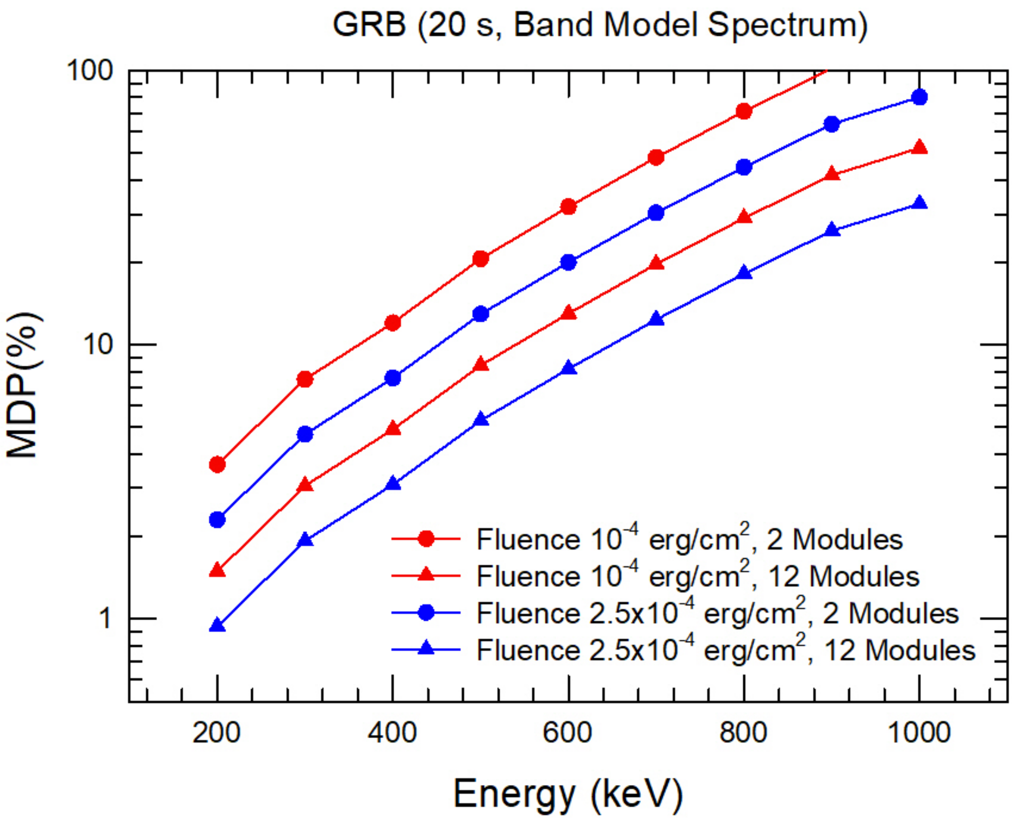

Figure 10: Minimum Detectable Polarization at 3σ level for a GRB of 20 s duration and 2 different fluences. The assumed spectrum is a Band law with low-energy photon index $\alpha = 1.0$, high energy photon index $\beta = 2.3$ and peak energy of the $EF(E)$ spectrum equal to 300 keV.

4.2.1 Laue lens

For a review on the physics underlying the Laue lenses see Frontera and von Ballmoos (2010). Briefly, Laue lenses exploit the crystal diffraction in transmission configuration (Laue geometry). A Laue lens is made of a large number of crystal tiles in transmission configuration,

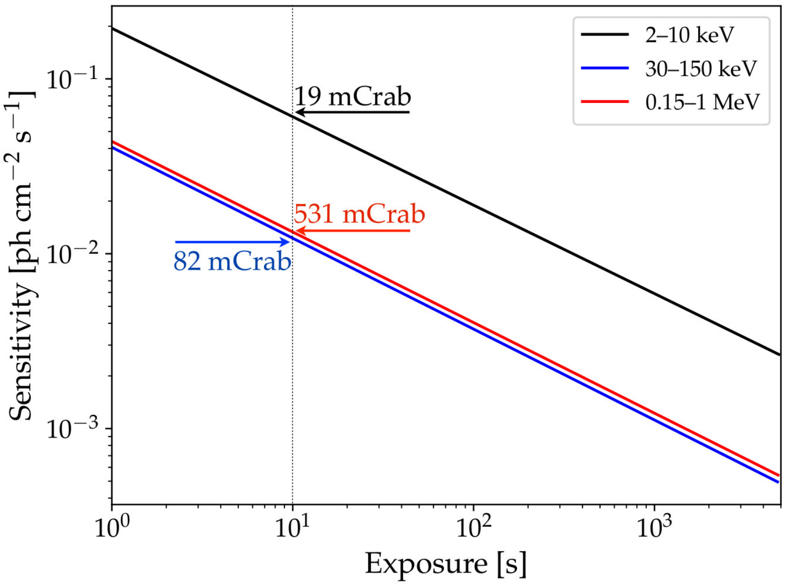

Figure 11: Continuum sensitivity of the WFM-IS in three energy bands, in the case of a source in the FoV of all detection units.

that are disposed in such a way that they concentrate the incident radiation onto a common focal spot. A convenient way to visualize the geometry of a crystal lens is to consider it as a spherical cup covered with rings of crystal tiles having their diffracting planes perpendicular to the sphere and the focal spot is on the symmetry axis at a focal distance $f = R/2$ from the cup, with R being the curvature radius of the spherical cup. From the Bragg law and the geometry of the lens, it can be easily demonstrated that the reflected energy from a crystal at distance r from the lens symmetry axis is given by (Frontera and von Ballmoos, 2010)

$$E = \frac{hc}{2d_{hkl}} \sin\left[\frac{1}{2}\arctan\left(\frac{f}{r}\right)\right] \approx \frac{hc\, f}{d_{hkl}\ r} \tag{1}$$

where d_{hkl} (in Å) is the distance between the chosen lattice planes (hkl Miller indices) of the crystals, $hc = 12.4$ keV·Å and E is the energy of the gamma-ray photon (in keV). The approximated expression is valid for gamma–ray lenses, given the small diffration angles involved. Thus the highest energies are diffracted from the nearest crystals and the lowest energies from the farest crystals to the lens axis. At the University of Ferrara, with the project HAXTEL (Hard X–ray TELescope) we developed a technology for assembling Laue lenses with moderate focal length (< 10 m), using flat mosaic crystal tiles of Copper Cu(111) (Frontera et al., 2008; Virgilli et al., 2011).

The disadvantage of flat crystals is that the minimum focal spot size is that of the crystal tiles. To overcome this limitation, bent crystals with the proper curvature are required. To this end, a technology for bending crystals and for assembling a Laue lens with long focal length (20 m) for astrophysical applications, was successfully developed as part of the LAUE project supported by the Italian Space Agency (ASI) (see, e.g, Virgilli et al. 2017). With the support of the European project AHEAD (integrated Activities in the High Energy Astrophysics Domain), the expected performance of a Laue lens prototype has also been simulated taking into account effects of possible crystal tile misalignments and radial distortions of the crystal curvature, as measured in laboratory experiments.

The lens under development is made of ∼19500 bent crystal tiles of Si(111) and Ge(111),

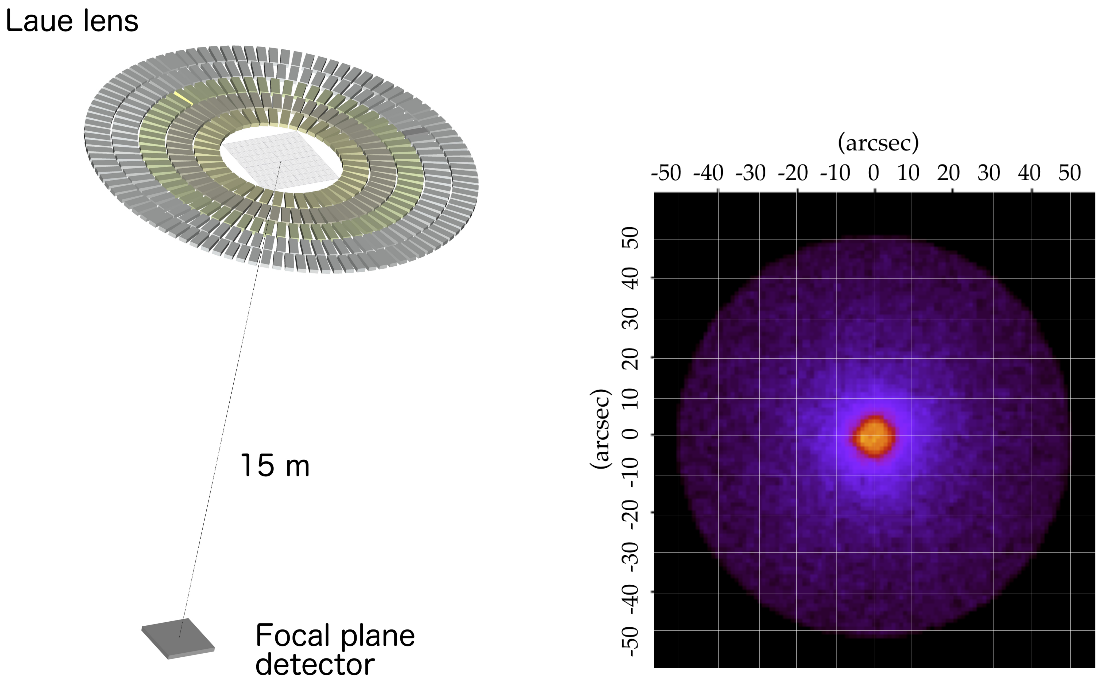

Figure 12: *Left*: Sketch of the Laue lens adopted for the Narrow Field Telescope (NFT) which will be made of bent crystals. The detector and the Laue lens dimensions are not to scale. *Right*: Simulated two-dimensional PSF image achieved with the NFT, as obtained with our Laue lens physical model with diffractive bent crystals, in the case of an on-axis source.

with 40 m curvature radius (within 5% uncertainty). In the current design the crystal tiles have a 30×10 mm^2 cross section, and a 2 mm thickness. Bent crystals have been produced and a technology for an accurate alignment (the requirement is a misalignment < 10 arcsec) of the crystal tiles in the lens has been identified (Virgilli et al., 2015) with successful results (paper in preparation). The development of a lens prototype is the goal of a recently approved project TRILL (Technological Readiness level Increase for Laue Lenses) devoted to increase the Technology Readiness Level (TRL). The Laue lens we propose for ASTENA builds on this recent technological progress. The expected Point Spread Function of the entire lens, validated by measurements on several subsets of crystals, is shown in the right panel of Fig 12, with a Half Energy Width (HEW) of 30 arcsec.

Important features of the proposed lens are its energy passband, angular resolution and Field of View (FOV). Thanks to the use of bent Si(111) and Ge(111) crystals tiles, an energy passband 50–600 keV is guaranteed; however we will explore the possibility to extend the energy band down to 30 keV, if the transparency of the passive materials in the lens under the crystals is still acceptable. Using simulations, validated by laboratory measurements on the performance of a large sample of bent crystals, we evaluated the angular resolution and FOV of the proposed lens. As shown in Fig. 13, an angular resolution of 0.5 arcmin can be achieved, with a useful FOV of approximately 4 arcmin.

4.2.2 Focal plane detector

The focal-plane detector is a solid state PSD made of 4 layers, with each layer made of 4×16 CdZnTe (CZT) elements. Each element is 2 cm thick with a cross section of 0.5×2 cm^2, which exhibits a drift strip configuration for the anodes and orthogonally segmented cathodes

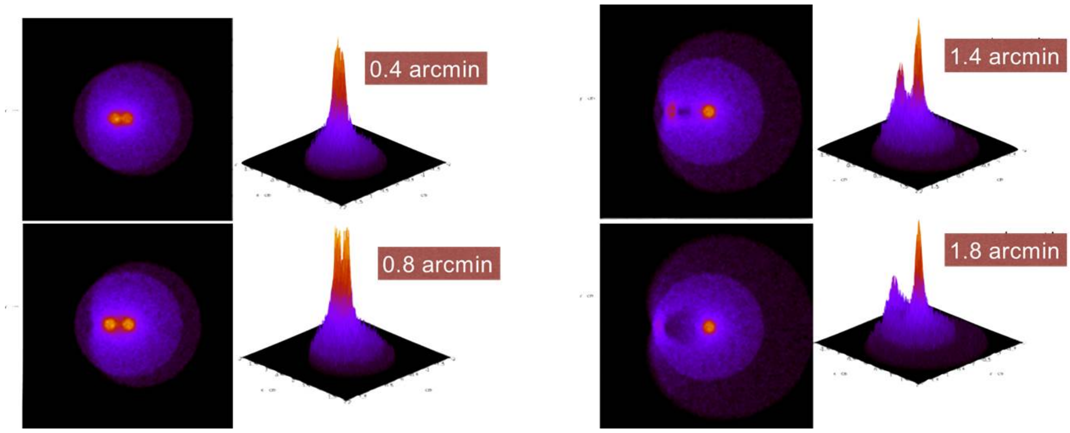

Figure 13: 2D and 3D PSF of the proposed lens in the case of two sources with different separations. One source is on-axis, while the other is located at increasing off-axis angles.

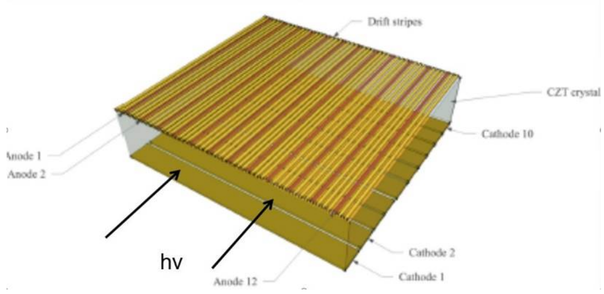

Figure 14: Strip configuration of a single detection element. The electric field is orthogonal to the incident photon direction.

in Parallel Transverse Field (PTF; see Fig. 14, Kuvvetli et al. 2014; Auricchio et al. 2012). The resulting PSD has a total cross section of 8×8 cm^2 and a total thickness of 8 cm. With this thickness, the PSD has a detection efficiency higher than 80% in the entire energy band of the NFT. The measured three-dimensional position resolution of a single element matches that required by the ASTENA NFT: 300 μm (Kuvvetli et al., 2010, 2014). In this configuration, the PSD is also capable to work as a Compton polarimeter (Caroli et al., 2018).

4.2.3 Expected NFT performance

- Sensitivity to continuum emission

  The expected NFT continuum sensitivity (3σ, 10^5 s, Δ E $= E/2$) is shown in Fig. 15, compared with that of other missions or experiments. This unprecedented sensitivity (up to two orders of magnitude better than operating instruments in the same energy band) is obtained thanks mainly to the use of properly bent crystals and to the transmission geometry, that allows a projected geometric area of about 7 m^2, with a very low mass of the lens ($\sim$ 150 kg).

- Sensitivity to polarized radiation

  The unprecedented sensitivity, together with the focal plane characteristics (high segmentation, spatial resolution in 3D and good energy resolution) will allow the NFT to enter a completely new territory in high-energy polarimetric measurements, making polarimetry a standard observation mode between 100 and 600/700 keV. To measure the

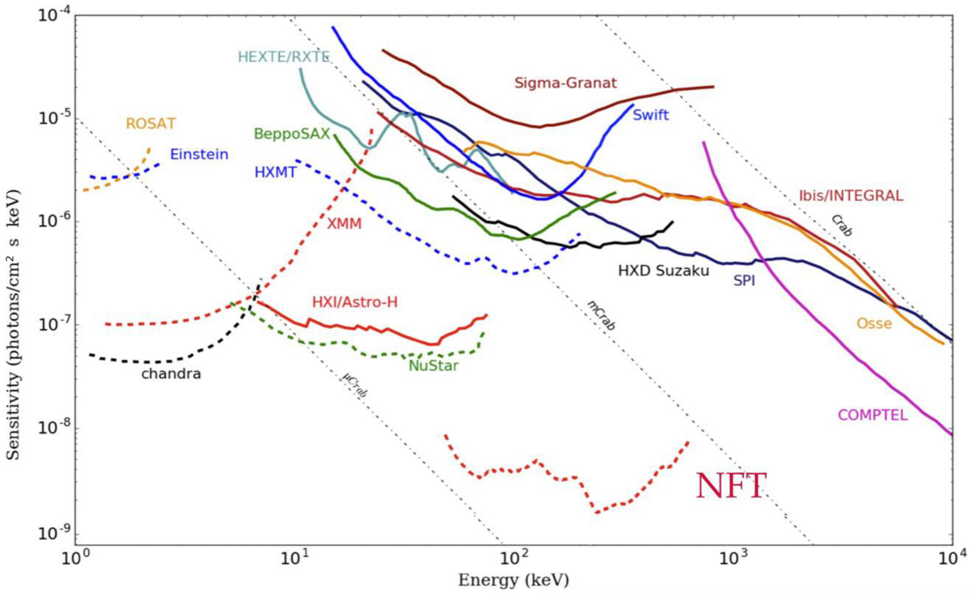

Figure 15: NFT continuum sensitivity at 3σ, with $\Delta E = E/2$ and Δ T $= 10^5$ s.

reliability of polarimetric measurements, we adopt the Minimum Detectable Polarization (MDP) parameter, which quantifies the confidence with which polarization is detected, i.e. that the source is not un-polarized. MDP should be significantly smaller than the degree of polarization to be measured. Following Weisskopf et al. (2006), the MDP at 99% confidence level can be expressed by

$$MDP_{99\%} = \frac{4.29}{A\,\epsilon\,S_F\,Q_{100}}\sqrt{\frac{A\,\epsilon\,S_F + B}{T}} \quad (2)$$

where, in the case of a focusing instrument, A is the effective area of the focusing telescope, ϵ is the detection efficiency (i.e., the double events efficiency for a scattering polarimeter), S_F is the source flux over the selected energy band (photons $\mathrm{cm}^{-2}\mathrm{s}^{-1}$), B is the background count rate (counts/s) integrated inside the volume of the detector subtended by the lens PSF, and T is the observation time. The factor Q_{100} is the polarimetric modulation factor of the detector (i.e., the measured modulation for a source 100% linearly polarized). The MDP achievable by the NFT can be estimated by evaluating the source count rate from the expected sensitivity reported in Fig. 15, in the energy band between 80 and 600 keV, and setting $Q_{100} = 0.6$. The latter is a realistic value for the NFT required focal plane, as can be inferred from different experiments performed using CdTe spectro-imagers operated as scattering polarimeters (Curado da Silva et al., 2008; Antier et al., 2015). Figure 16 shows this estimate as a function of both the observing time for a 10 mCrab source, and the source intensity integrated over 10^5 s. A Crab-like spectrum is assumed, with a background level given by Dean et al. (1989) and later confirmed with the INTEGRAL SPI instrument, scaled to a low earth orbit. These results confirm unprecedented polarimetric performance of the NFT telescope with an achievable MDP of 5% for a 10mCrab source for a 10^5 s observation time.

- Sensitivity to narrow emission lines

  In general, for a focusing telescope, the sensitivity to a narrow emission line expressed

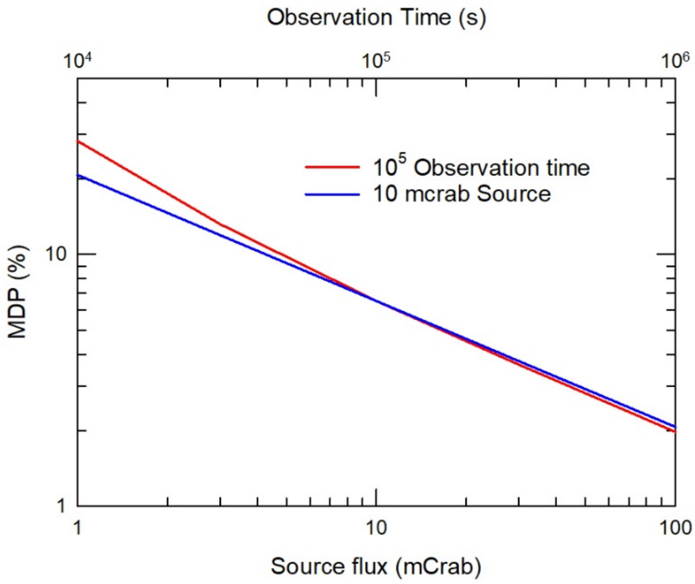

Figure 16: Minimum Detectable Polarization (MDP) in 10^5 s as a function of the polarized source intensity (*red line*) and for a 10 mCrab source as a function of the observation time (*blue line*). In both cases, we assumed a modulation factor of the detector $Q_{100} = 0.6$.

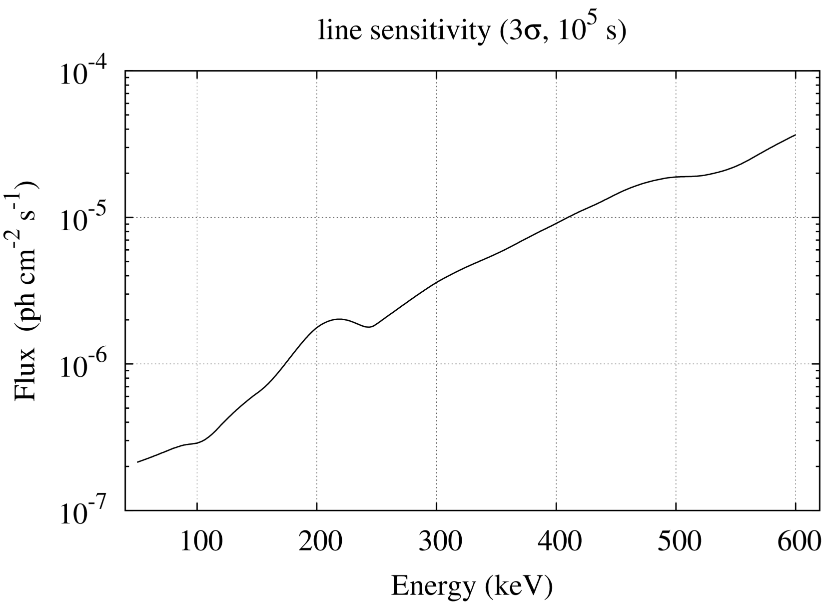

Figure 17: Expected line sensitivity for the NFT on board ASTENA, calculated for an observation time of 10^5 s, at 3 σ confidence level.

in photons/(cm^2 s), superimposed onto a continuum source spectrum, at a confidence level of n_σ, is given by:

$$I_L^{min}(E_l) = 1.31 n_\sigma \frac{\sqrt{[2B(E_l)A_d + I_c(E_l)\eta_d f_\epsilon A_{eff}]\Delta E}}{\eta_d f_\epsilon A_{eff}\sqrt{T_{obs}}} \tag{3}$$

where E$_L$ is the line centroid,$I_c(E_L)$ is the source continuum intensity at the line centroid, ΔE is the FWHM of the line profile that depends upon the energy resolution of the detector which has been assumed to be 2 keV (expected for our simulated detector Khalil et al. 2015). The other parameters, all calculated at the energy E_L, are those defined above.

The sensitivity to an emission line for our Laue lens, at 3σ confidence level, is shown in Fig. 17 for an observation time of 10^5 s. Here we have adopted a typical scatter of the radial curvature of bent crystals (Gaussian deviation of 2.5% from the mean) and a tile misalignment within 10 arcsec; a continuum intensity given by our continuum sensitivity, a FWHM of the line of 2 keV and the fraction $f_\epsilon = 0.5$, corresponding to a half energy width of the PSF. This figure shows how the line sensitivity of the ASTENA/NFT in 10^5 s is approximately three orders of magnitude better then the SPI instrument aboard INTEGRAL at low energy, while it is about one order of magnitude better at 511 keV [3]. This sensitivity can be further improved with a suitable choice and configuration of the reflecting planes of bent crystals in the lens.

In the common pass-band, a comparison of these performances with the NASA Medium Probe design mission AMEGO (McEnery et al., 2019) shows that ASTENA has a much higher sensitivity at low energies, while at 511 keV ASTENA's sensitivity is similar, but with an order of magnitude better angular resolution.

[3] `https://www.cosmos.esa.int/web/integral/observation-time-estimator`, see also Siegert et al. (2016)

References

I. Ahmad, J. P. Greene, E. F. Moore, S. Ghelberg, A. Ofan, M. Paul, and W. Kutschera. Improved measurement of the Ti44 half-life from a 14-year long study. *Phys. Rev. C*, 74(6): 065803, Dec. 2006. doi: 10.1103/PhysRevC.74.065803.

F. Albernhe, J. F. Le Borgne, G. Vedrenne, D. Boclet, P. Durouchoux, and J. M. da Costa. Detection of the positron annihilation gamma ray line from the Galactic Center region. *A&A*, 94(2):214–218, Feb 1981.

A. Alexis, P. Jean, P. Martin, and K. Ferrière. Monte Carlo modelling of the propagation and annihilation of nucleosynthesis positrons in the Galaxy. *arXiv.org*, 564:A108, Apr. 2014.

S. Antier, P. Ferrando, O. Limousin, E. Caroli, R. M. Curado da Silva, and et al. Hard X-ray polarimetry with Caliste, a high performance CdTe based imaging spectrometer. *Experimental Astronomy*, 39:233–258, June 2015. doi: 10.1007/s10686-015-9442-5.

N. Auricchio, E. Caroli, A. Basili, and et al. Development status of a CZT spectrometer prototype with 3D spatial resolution for hard x-ray astronomy. In *High Energy, Optical, and Infrared Detectors for Astronomy V*, volume 8453 of *Proc. SPIE*, page 84530S, July 2012. doi: 10.1117/12.928327.

R. M. Bandyopadhyay, J. Silk, J. E. Taylor, and T. J. Maccarone. On the origin of the 511-keV emission in the Galactic Centre. *MNRAS*, 392:1115–1123, Jan. 2009.

R. Bartels, F. Calore, E. Storm, and C. Weniger. Galactic binaries can explain the Fermi Galactic centre excess and 511 keV emission. *arXiv.org*, 480:3826–3841, Nov. 2018.

G. S. Bisnovatyi-Kogan and A. S. Pozanenko. Can Flare Stars Explain the Annihilation Line from the Galactic Bulge? *Astrophysics*, 60(2):223–227, June 2017.

C. Bœhm. The dark matter interpretation of the 511 keV line. *New Journal of Physics*, 11 (10):105009, oct 2009. doi: 10.1088/1367-2630/11/10/105009.

C. Boehm, D. Hooper, J. Silk, M. Casse, and J. Paul. Mev dark matter: Has it been detected? *Phys. Rev. Lett.*, 92:101301, Mar 2004. doi: 10.1103/PhysRevLett.92.101301.

S. E. Boggs, F. A. Harrison, H. Miyasaka, B. W. Grefenstette, and et al. ^{44}Ti gamma-ray emission lines from SN1987A reveal an asymmetric explosion. *Science*, 348(6235):670–671, May 2015. doi: 10.1126/science.aaa2259.

L. Bouchet, P. Mandrou, J. P. Roques, G. Vedrenne, and et al. SIGMA Discovery of Variable E +- E - Annihilation Radiation from the Near Galactic Center Variable Compact Source 1E 1740.7-2942. *ApJ*, 383:L45, Dec 1991. doi: 10.1086/186237.

L. Bouchet, A. Strong, E. Jourdain, J. P. Roques, T. Porter, I. Moskalenko, R. Diehl, and E. Orlando. A complete all-sky survey with INTEGRAL/SPI: sources census, hard X-ray diffuse emission and annihilation line. In *The Extreme Sky: Sampling the Universe above 10 keV*, page 16, 2009.

R. Campana, F. Fuschino, C. Labanti, L. Amati, S. Mereghetti, M. Fiorini, F. Frontera, G. Baldazzi, P. Bellutti, and et al. The X-Gamma Imaging Spectrometer (XGIS) onboard THESEUS . *Mem. Soc. Astron. Italiana*, 89:137, 2018.

E. Caroli, M. Moita, R. da Silva, S. Del Sordo, G. de Cesare, J. Maia, and M. Pàscoa. Hard X-ray and Soft Gamma Ray Polarimetry with CdTe/CZT Spectro-Imager. *Galaxies*, 6:69, July 2018. doi: 10.3390/galaxies6030069.

E. Cavallari and F. Frontera. Hard X-Ray/Soft Gamma-Ray Experiments and Missions: Overview and Prospects. *Space Sci. Rev.*, 212:429–518, Oct. 2017. doi: 10.1007/s11214-017-0426-9.

A. Celotti and R. D. Blandford. On the Formation of Jets. In L. Kaper, E. P. J. V. D. Heuvel, and P. A. Woudt, editors, *Black Holes in Binaries and Galactic Nuclei*, page 206, 2001.

M. H. Chan and C. H. Leung. Constraining dark matter by the 511 keV line. *MNRAS*, 479 (2):2229–2234, Sep 2018. doi: 10.1093/mnras/sty1583.

E. Churazov, R. Sunyaev, S. Sazonov, M. Revnivtsev, and D. Varshalovich. Positron annihilation spectrum from the Galactic Centre region observed by SPI/INTEGRAL. *MNRAS*, 357(4):1377–1386, Mar 2005. doi: 10.1111/j.1365-2966.2005.08757.x.

E. Churazov, R. Sunyaev, J. Isern, J. Knödlseder, P. Jean, F. Lebrun, N. Chugai, S. Grebenev, E. Bravo, S. Sazonov, and M. Renaud. Cobalt-56 γ-ray emission lines from the type Ia supernova 2014J. *Nature*, 512:406–408, Aug. 2014. doi: 10.1038/nature13672.

D. a. . Clayton. Introduction. *ApJ*, 155:75, Mar 1969. doi: 10.1086/149849.

D. D. Clayton and F. Hoyle. Gamma-Ray Lines from Novae. *ApJ*, 187:L101, Feb. 1974. doi: 10.1086/181406.

R. M. Curado da Silva, E. Caroli, J. B. Stephen, and et al. Polarimetric performance of a Laue lens gamma-ray CdZnTe focal plane prototype. *Journal of Applied Physics*, 104(8): 084903–084903, Oct. 2008. doi: 10.1063/1.3000092.

J. K. Daugherty and A. K. Harding. Pair production in superstrong magnetic fields. *apj*, 273: 761–773, Oct. 1983. doi: 10.1086/161411.

A. J. Dean, L. Fan, K. Byard, A. Goldwurm, and C. J. Hall. The gamma-ray emissivity of the earth's atmosphere. *A&A*, 219:358–361, July 1989.

R. Diehl. Gamma rays from a supernova of type Ia: SN2014J. *Astronomische Nachrichten*, 336(5):464, Jun 2015. doi: 10.1002/asna.201512179.

R. Diehl, T. Siegert, W. Hillebrandt, and et al. Early ^{56}Ni decay gamma rays from SN2014J suggest an unusual explosion. *Science*, 345(6201):1162–1165, Sep 2014. doi: 10.1126/science.1254738.

D. P. Finkbeiner and N. Weiner. Exciting dark matter and the integral/spi 511 kev signal. *Phys. Rev. D*, 76:083519, Oct 2007. doi: 10.1103/PhysRevD.76.083519. URL `https://link.aps.org/doi/10.1103/PhysRevD.76.083519`.

F. Frontera and P. von Ballmoos. Laue Gamma-Ray Lenses for Space Astrophysics: Status and Prospects. *X-Ray Optics and Instrumentation, 2010. Special Issue on X-Ray Focusing: Techniques and Applications, id.215375*, 2010:215375, 2010. doi: 10.1155/2010/215375.

F. Frontera, E. Costa, D. dal Fiume, M. Feroci, L. Nicastro, M. Orlandini, E. Palazzi, and G. Zavattini. The high energy instrument PDS on-board the BeppoSAX X–ray astronomy satellite. *Astronomy and Astrophysics Suppl. Series*, 122:357–369, Apr. 1997. doi: 10.1051/aas:1997140.

F. Frontera, G. Loffredo, A. Pisa, F. Nobili, V. Carassiti, F. Evangelisti, L. Landi, S. Squerzanti, E. Caroli, J. B. Stephen, K. H. Andersen, P. Courtois, N. Auricchio, L. Milani, and B. Negri. Focusing of gamma-rays with Laue lenses: first results. In *Society of Photo-Optical Instrumentation Engineers (SPIE) Conference Series*, volume 7011, 2008.

N. Gehrels, S. D. Barthelmy, B. J. Teegarden, J. Tueller, M. Leventhal, and C. J. MacCallum. GRIS observations of positron annihilation radiation from the Galactic center. *ApJ*, 375: L13–L16, July 1991. doi: 10.1086/186077.

A. Goldwurm, J. Ballet, B. Cordier, J. Paul, L. Bouchet, J. P. Roques, D. Barret, P. Mandrou, R. Sunyaev, E. Churazov, M. Gilfanov, A. Dyachkov, N. Khavenson, V. Kovtunenko, R. Kremnev, and K. Sukhanov. Sigma/GRANAT soft gamma-ray observations of the X-ray nova in Musca - Discovery of positron annihilation emission line. *The Astrophysical Journal Letters*, 389:L79–L82, Apr. 1992.

J. Gómez-Gomar, J. Isern, and P. Jean. Prospects for Type IA supernova explosion mechanism identification with gamma rays. *MNRAS*, 295:1–9, Mar. 1998. doi: 10.1046/j.1365-8711.1998.29511115.x.

S. A. Grebenev, A. A. Lutovinov, S. S. Tsygankov, and C. Winkler. Hard-X-ray emission lines from the decay of ^{44}Ti in the remnant of supernova 1987A. *Nature*, 490:373–375, Oct. 2012. doi: 10.1038/nature11473.

B. W. Grefenstette, F. A. Harrison, S. E. Boggs, S. P. Reynolds, C. L. Fryer, and et al. Asymmetries in core-collapse supernovae from maps of radioactive ^{44}Ti in CassiopeiaA. *Nature*, 506:339–342, Feb. 2014. doi: 10.1038/nature12997.

B. W. Grefenstette, C. L. Fryer, F. A. Harrison, S. E. Boggs, and et al. The Distribution of Radioactive ^{44}Ti in Cassiopeia A. *ApJ*, 834:19, Jan. 2017. doi: 10.3847/1538-4357/834/1/19.

C. J. Hailey, K. Mori, F. E. Bauer, M. E. Berkowitz, J. Hong, and B. J. Hord. A density cusp of quiescent X-ray binaries in the central parsec of the Galaxy. *Nature*, 556:70–73, Apr. 2018. doi: 10.1038/nature25029.

F. A. Harrison, W. W. Craig, F. E. Christensen, C. J. Hailey, W. W. Zhang, and et al. The Nuclear Spectroscopic Telescope Array (NuSTAR) High-energy X-Ray Mission. *The Astrophysical Journal*, 770:103, June 2013.

J. Isern, P. Jean, E. Bravo, J. Knödlseder, and et al. Gamma-ray emission from SN2014J near maximum optical light. *A&A*, 588:A67, Apr 2016. doi: 10.1051/0004-6361/201526941.

P. Jean, J. Knödlseder, W. Gillard, and et al. Spectral analysis of the Galactic e^+e^- annihilation emission. *Astronomy & Astrophysics*, 445(2):579–589, Jan. 2006.

W. N. Johnson, III, F. R. Harnden, Jr., and R. C. Haymes. The Spectrum of Low-Energy Gamma Radiation from the Galactic-Center Region. *ApJ*, 172:L1, Feb. 1972. doi: 10.1086/180878.

M. Khalil, F. Frontera, E. Caroli, E. Virgilli, and V. Valsan. A simulation study on the focal plane detector of the LAUE project. *Nuclear Instruments and Methods in Physics Research A*, 786:59–70, June 2015. doi: 10.1016/j.nima.2015.03.004.

J. Knödlseder, P. Jean, V. Lonjou, G. Weidenspointner, N. Guessoum, W. Gillard, G. Skinner, P. von Ballmoos, G. Vedrenne, J.-P. Roques, S. Schanne, B. Teegarden, V. Schönfelder, and C. Winkler. The all-sky distribution of 511 keV electron-positron annihilation emission. *A&A*, 441:513–532, Oct. 2005. doi: 10.1051/0004-6361:20042063.

O. Korobkin, A. M. Hungerford, C. L. Fryer, M. R. Mumpower, G. W. Misch, T. M. Sprouse, J. Lippuner, R. Surman, A. J. Couture, P. F. Bloser, F. Shirazi, W. P. Even, W. T. Vestrand, and R. S. Miller. Gamma-rays from kilonova: a potential probe of r-process nucleosynthesis. *arXiv e-prints*, art. arXiv:1905.05089, May 2019.

M. J. Kuchner, R. P. Kirshner, P. A. Pinto, and B. Leibundgut. Evidence for Ni-56 yields Co-56 yields Fe-56 decay in type IA supernovae. *ApJ*, 426:89–92, May 1994. doi: 10.1086/187347.

I. Kuvvetli, C. Budtz-Jørgensen, E. Caroli, and N. Auricchio. CZT drift strip detectors for high energy astrophysics. *Nuclear Instruments and Methods in Physics Research A*, 624: 486–491, Dec. 2010. doi: 10.1016/j.nima.2010.03.172.

I. Kuvvetli, C. Budtz-Jørgensen, A. Zappettini, and et al. A 3D CZT high resolution detector for x- and gamma-ray astronomy. In *High Energy, Optical, and Infrared Detectors for Astronomy VI*, volume 9154 of *Proc. SPIE*, page 91540X, July 2014. doi: 10.1117/12.2055119.

M. Leventhal, C. J. MacCallum, and P. D. Stang. Detection of 511 keV positron annihilation radiation from the galactic center direction. *ApJ*, 225:L11–L14, Oct. 1978. doi: 10.1086/182782.

M. Leventhal, C. J. MacCallum, A. F. Huters, and P. D. Stang. Gamma-ray lines and continuum radiation from the galactic center direction. *ApJ*, 240:338–343, Aug. 1980. doi: 10.1086/158237.

M. Leventhal, C. J. MacCallum, A. F. Huters, and P. D. Stang. Current status of the galactic center positron-annihilation source. *ApJ*, 302:459–461, Mar. 1986. doi: 10.1086/164004.

R. E. Lingenfelter and R. Ramaty. The Nature of the Annihilation Radiation and Gamma-Ray Continuum from the Galactic Center Region. *ApJ*, 343:686, Aug 1989. doi: 10.1086/167740.

M. Marisaldi, C. Labanti, and H. Soltau. A Pulse Shape Discrimination Gamma-Ray Detector Based on a Silicon Drift Chamber Coupled to a CsI(Tl) Scintillator: Prospects for a 1 keV 1 MeV Monolithic Detector. *IEEE Transactions on Nuclear Science*, 51:1916–1922, Aug. 2004. doi: 10.1109/TNS.2004.832679.

M. Marisaldi, C. Labanti, H. Soltau, C. Fiorini, A. Longoni, and F. Perotti. X- and Gamma-Ray Detection With a Silicon Drift Detector Coupled to a CsI(Tl) Scintillator Operated With Pulse Shape Discrimination Technique. *IEEE Transactions on Nuclear Science*, 52: 1842–1848, Oct. 2005. doi: 10.1109/TNS.2005.856615.

J. McEnery, J. Abel Barrio, I. Agudo, and et al. All-sky Medium Energy Gamma-ray Observatory: Exploring the Extreme Multimessenger Universe. *arXiv e-prints*, art. arXiv:1907.07558, Jul 2019.

P. A. Milne, L. S. The, and M. D. Leising. Positron Escape from Type IA Supernovae. *ApJS*, 124(2):503–526, Oct 1999. doi: 10.1086/313262.

P. e. a. . Mroz. Clasical nova systems. *ApJS*, 219:26, Mar 2015. doi: 10.1088/0067-0049/219/2/26.

M. M. Phillips. The absolute magnitudes of Type IA supernovae. *ApJ*, 413:L105–L108, Aug. 1993. doi: 10.1086/186970.

N. Prantzos, C. Boehm, A. M. Bykov, R. Diehl, K. Ferrière, N. Guessoum, P. Jean, J. Knoedlseder, A. Marcowith, I. V. Moskalenko, A. Strong, and G. Weidenspointner. The 511 keV emission from positron annihilation in the Galaxy. *Reviews of Modern Physics*, 83: 1001–1056, July 2011. doi: 10.1103/RevModPhys.83.1001.

W. R. Purcell, D. A. Grabelsky, M. P. Ulmer, W. N. Johnson, R. L. Kinzer, J. D. Kurfess, M. S. Strickman, and G. V. Jung. OSSE observations of Galactic 511 keV positron annihilation radiation - Initial phase 1 results. *ApJ*, 413:L85–L88, Aug. 1993. doi: 10.1086/186965.

W. R. Purcell, L.-X. Cheng, D. D. Dixon, R. L. Kinzer, J. D. Kurfess, M. Leventhal, M. A. Saunders, J. G. Skibo, D. M. Smith, and J. Tueller. OSSE Mapping of Galactic 511 keV Positron Annihilation Line Emission. *ApJ*, 491:725–748, Dec. 1997.

M. Renaud, J. Vink, A. Decourchelle, F. Lebrun, and et al. The Signature of ^{44}Ti in Cassiopeia A Revealed by IBIS/ISGRI on INTEGRAL. *ApJ*, 647:L41–L44, Aug. 2006. doi: 10.1086/507300.

G. H. Share, M. D. Leising, D. C. Messina, and W. R. Purcell. Limits on a variable source of 511 keV annihilation radiation near the Galactic center. *ApJ*, 358:L45–L48, Aug. 1990. doi: 10.1086/185776.

T. Siegert, R. Diehl, M. G. H. Krause, and J. Greiner. Revisiting INTEGRAL/SPI observations of ^{44}Ti from Cassiopeia A. *A&A*, 579:A124, Jul 2015. doi: 10.1051/0004-6361/201525877.

T. Siegert, R. Diehl, J. Greiner, M. G. H. Krause, A. M. Beloborodov, M. C. Bel, F. Guglielmetti, J. Rodriguez, A. W. Strong, and X. Zhang. Positron annihilation signatures associated with the outburst of the microquasar V404 Cygni. *Nature*, 531:341–343, Mar. 2016a. doi: 10.1038/nature16978.

T. Siegert, R. Diehl, G. Khachatryan, M. G. H. Krause, F. Guglielmetti, J. Greiner, A. W. Strong, and X. Zhang. Gamma-ray spectroscopy of positron annihilation in the Milky Way. *Astronomy and Astrophysics*, 586:A84, Feb. 2016b. doi: 10.1051/0004-6361/201527510.

T. Siegert, R. Diehl, A. C. Vincent, F. Guglielmetti, M. G. H. Krause, and C. Boehm. Search for 511 keV emission in satellite galaxies of the Milky Way with INTEGRAL/SPI. *arXiv.org*, 595:A25, Oct. 2016.

T. Siegert, R. M. Crocker, R. Diehl, M. G. H. Krause, F. H. Panther, M. M. M. Pleintinger, and C. Weinberger. Constraints on positron annihilation kinematics in the inner Galaxy. *Astronomy & Astrophysics*, 627:A126, July 2019.

S. A. Sim and P. A. Mazzali. On the γ-ray emission of Type Ia supernovae. *MNRAS*, 385: 1681–1690, Apr. 2008. doi: 10.1111/j.1365-2966.2008.12600.x.

G. Skinner, R. Diehl, X. Zhang, L. Bouchet, and P. Jean. The Galactic distribution of the 511 keV e^+/e^- annihilation radiation. In *Proceedings of the 10th INTEGRAL Workshop: "A Synergistic View of the High-Energy Sky" (INTEGRAL 2014). 15-19 September 2014. Annapolis, MD, USA. Published online at http://pos.sissa.it/cgi-bin/reader/conf.cgi?confid=228, id.054*, page 054, 2014.

B. J. Teegarden, T. L. Cline, N. Gehrels, D. Palmer, R. Ramaty, H. Seifert, K. H. Hurley, D. A. Landis, N. W. Madden, D. Malone, R. Pehl, and A. Owens. TGRS Observation of the Galactic Center Annihilation Line. *apj letter*, 463:L75, June 1996. doi: 10.1086/310061.

F. Timmes, C. Fryer, F. Timmes, A. L. Hungerford, A. Couture, F. Adams, W. Aoki, A. Arcones, D. Arnett, K. Auchettl, and et al. Catching Element Formation In The Act ; The Case for a New MeV Gamma-Ray Mission: Radionuclide Astronomy in the 2020s. In *BAAS*, volume 51, page 2, May 2019.

G. Vedrenne, J.-P. Roques, V. Schönfelder, P. Mandrou, G. G. Lichti, and et al. SPI: The spectrometer aboard INTEGRAL. *Astronomy and Astrophysics*, 411:L63–L70, Nov. 2003.

J. Vink, J. M. Laming, J. S. Kaastra, J. A. M. Bleeker, and et al. Detection of the 67.9 and 78.4 keV Lines Associated with the Radioactive Decay of ^{44}Ti in Cassiopeia A. *ApJ*, 560: L79–L82, Oct. 2001. doi: 10.1086/324172.

E. Virgilli, F. Frontera, V. Valsan, V. Liccardo, V. Carassiti, F. Evangelisti, and S. Squerzanti. Laue lenses for hard x-/soft γ-rays: new prototype results. In *Society of Photo-Optical Instrumentation Engineers (SPIE) Conference Series*, volume 8147 of *Proc. SPIE*, page 81471B, Sept. 2011. doi: 10.1117/12.895233.

E. Virgilli, F. Frontera, P. Rosati, V. Liccardo, S. Squerzanti, V. Carassiti, E. Caroli, N. Auricchio, and J. B. Stephen. Hard x-ray broad band Laue lenses (80-600 keV): building methods and performances. In *Society of Photo-Optical Instrumentation Engineers (SPIE) Conference Series*, volume 9603 of *Proc. SPIE*, page 960308, Sept. 2015. doi: 10.1117/12.2190335.

E. Virgilli, V. Valsan, F. Frontera, E. Caroli, V. Liccardo, and J. B. Stephen. Expected performances of a Laue lens made with bent crystals. *Journal of Astronomical Telescopes, Instruments, and Systems*, 3(4):044001, Oct. 2017. doi: 10.1117/1.JATIS.3.4.044001.

G. Weidenspointner, G. Skinner, P. Jean, J. Knödlseder, P. von Ballmoos, G. Bignami, R. Diehl, A. W. Strong, B. Cordier, S. Schanne, and C. Winkler. An asymmetric distribution of positrons in the Galactic disk revealed by γ-rays. *nature*, 451:159–162, Jan. 2008. doi: 10.1038/nature06490.

M. C. Weisskopf, R. F. Elsner, D. Hanna, V. M. Kaspi, S. L. O'Dell, G. G. Pavlov, and B. D. Ramsey. The prospects for X-ray polarimetry and its potential use for understanding neutron stars. *arXiv Astrophysics e-prints*, Nov. 2006.

R. J. Wilkinson, A. C. Vincent, C. BÅ‘hm, and C. McCabe. Ruling out the light weakly interacting massive particle explanation of the Galactic 511 keV line. *Phys. Rev. D*, 94(10): 103525, Nov 2016. doi: 10.1103/PhysRevD.94.103525.

M.-R. Wu, P. Banerjee, B. D. Metzger, G. Martínez-Pinedo, T. Aramaki, E. Burns, C. J. Hailey, J. Barnes, and G. Karagiorgi. Finding the remnants of the Milky Way's last neutron star mergers. *arXiv e-prints*, art. arXiv:1905.03793, May 2019.